Title
A new mechanism for ozonolysis of unsaturated organics on solids: phosphocholines on NaCl as a model for sea salt particles.

Journal
Physical chemistry chemical physics : PCCP, 10(4)

ISSN
1463-9076

Authors
Karagulian, Federico
Scott Lea, A
Dilbeck, Christopher W
et al.

Publication Date
2008-01-28

Peer reviewed

PCCP

Physical Chemistry Chemical Physics

www.rsc.org/pccp

Volume 10 | Number 4 | 28 January 2008 | Pages 461–608

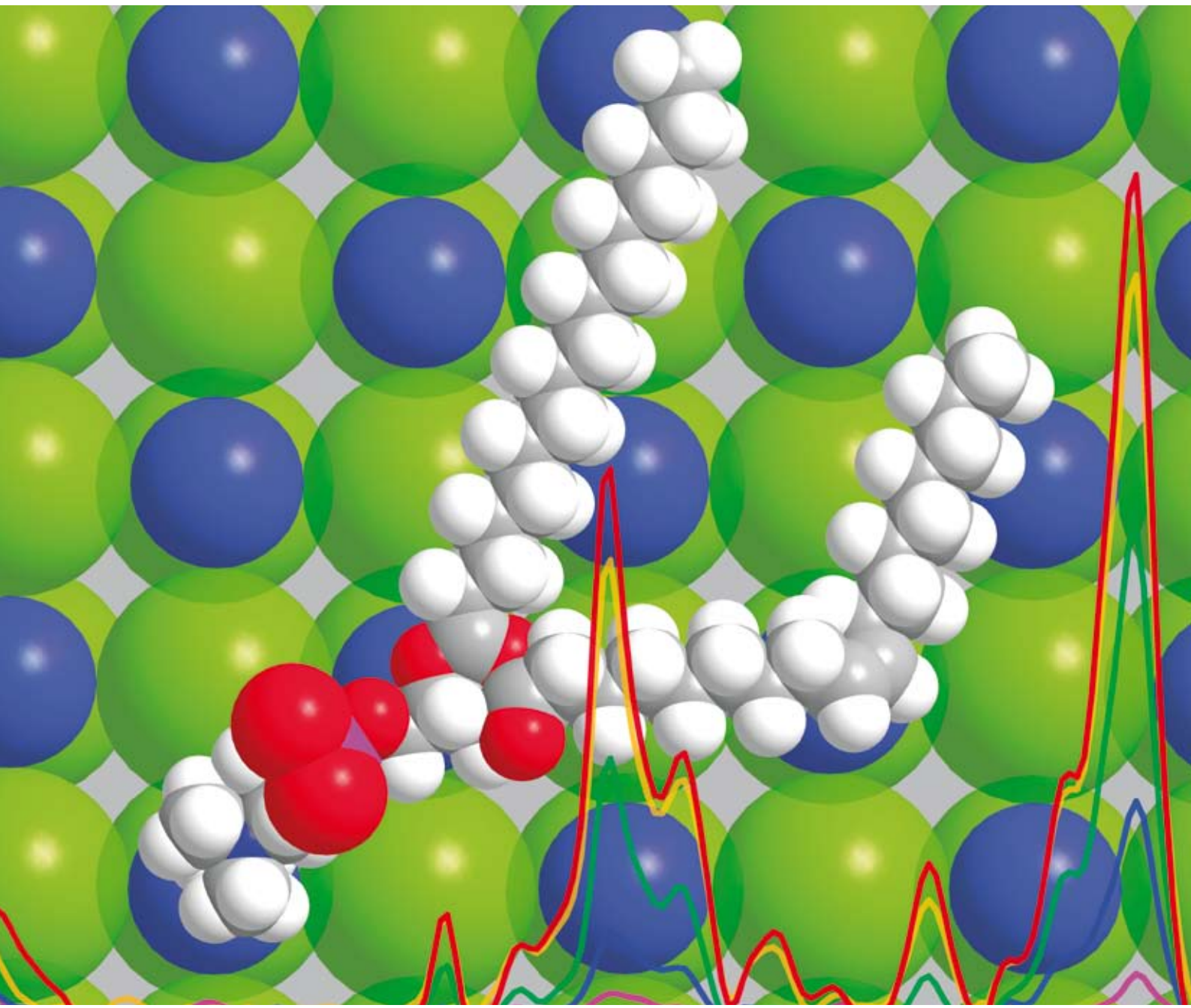

ISSN 1463-9076

COVER ARTICLE
Finlayson-Pitts *et al.*
A new mechanism for ozonolysis of unsaturated organics on solids: phosphocholines on NaCl as a model for sea salt particles

PERSPECTIVE
Lischka *et al.*
Nonadiabatic excited-state dynamics of polar π-systems and related model compounds of biological relevance

RSC Publishing

1463-9076(2008)10:4;1-9

A new mechanism for ozonolysis of unsaturated organics on solids: phosphocholines on NaCl as a model for sea salt particles

Federico Karagulian,[a] A. Scott Lea,[b] Christopher W. Dilbeck[a] and Barbara J. Finlayson-Pitts*[a]

Received 17th August 2007, Accepted 13th November 2007
First published as an Advance Article on the web 4th December 2007
DOI: 10.1039/b712715d

The ozonolysis of an approximately one monolayer film of 1-oleoyl-2-palmitoyl-*sn*-glycero-3-phosphocholine (OPPC) on NaCl was followed in real time using diffuse reflection infrared Fourier transform spectrometry (DRIFTS) at 23 °C. Matrix-assisted laser desorption/ionization (MALDI) mass spectrometry and Auger electron spectroscopy were used to confirm the identification of the products. Ozone concentrations ranged from 1.7×10^{12} to 7.0×10^{13} molecules cm^{-3} (70 ppb to 2.8 ppm). Upon exposure to O_3, there was a loss of C=C accompanied by the formation of a strong band at $\sim$1110 cm^{-1} due to the formation of a stable secondary ozonide (1,2,4-trioxolane, SOZ). The yield of the SOZ was smaller when the reaction was carried out in the presence of water vapor at concentrations corresponding to relative humidities between 2 and 25%. The dependencies of the rate of SOZ formation on the concentrations of ozone and water vapor are consistent with the initial formation of a primary ozonide (1,2,3-trioxolane, POZ) that can react with O_3 or H_2O in competition with its thermal decomposition to a Criegee intermediate and aldehyde. Estimates were obtained for the rate constants for the POZ thermal decomposition and for its reactions with O_3 and H_2O, as well as for the initial reaction of O_3 with OPPC. The SOZ decomposed upon photolysis in the actinic region generating aldehydes, carboxylic acids and anhydrides. These studies show that the primary ozonide has a sufficiently long lifetime when formed on a solid substrate that direct reactions with O_3 and H_2O can compete with its thermal decomposition. In dry polluted atmospheres, ozone–alkene reactions may lead in part to the formation of stable secondary ozonides whose chemistry, photochemistry and toxicity should be taken into account in models of such regions.

Introduction

Sea salt particles are a major contributor to the global aerosol burden.[1–4] They are formed by wave action, which carries along organic material with the sea salt. Tervahattu and coworkers, for example, used TOF-SIMS to show that palmitic acid and other fatty acids are associated with marine aerosol particles.[5,6] A major source of this organic layer is the decomposition of marine organisms, which have biomembranes that are a mixture of lipids, hydrophobic proteins and carbohydrates.[7,8] Phospholipids and fatty acids (mainly C_{12-18}) are common products of biomembrane disintegration.[9,10] Previous work has indicated that fatty acid lipids in sea salt particles can be enhanced by factors of (5–9) $\times 10^4$ compared to ocean surface water.[10] In addition to the material from biomembranes, bacteria can also be enriched on the particle surfaces.[11,12]

An organic coating on sea salt particles is expected to modify the chemical and physical properties of the particles including their radiative properties.[8,13–16] For example, it could affect the uptake of gases such as water,[17] altering both the gas and particle phases. Such effects on the particle properties may also change upon oxidation of the organic layer.

We report here studies of the oxidation of an unsaturated phospholipid, 1-oleoyl-2-palmitoyl-*sn*-glycero-3-phosphocholine (OPPC), adsorbed on NaCl as a model for lipids on sea salt. The choice is based on the fact that phosphocholines constitute the most abundant class of phospholipids, and that palmitic and oleic acids are two of the most common fatty acid components of the phospholipids. The reaction was followed in real time using diffuse reflection infrared Fourier transform spectrometry (DRIFTS).[18–20] Matrix-assisted laser desorption/ionization (MALDI) mass spectrometry and Auger electron spectroscopy were used to confirm the identification of the products and to provide additional insights into the chemistry. We show that the primary ozonide formed in the reaction has a sufficiently long lifetime that it can react with other species such as O_3 or H_2O in competition with its thermal decomposition. To the best of our knowledge, this is the first such observation, and suggests an additional route for the formation of secondary ozonides on surfaces in polluted and relatively dry environments.

[a] *Department of Chemistry, University of California, Irvine, California, 92697-2025. E-mail: bjfinlay@uci.edu; Fax: (949) 824-2420; Tel: (949) 824-7670*
[b] *W.R. Wiley Environmental Science Laboratory, Pacific Northwest National Laboratory, Richland, Washington, 99352*

Experimental

Sample preparation

NaCl powders were prepared by grinding crystalline NaCl (Sigma Aldrich, 99.5%) in a Wig-L-Bug (Crescent Dental Manufacturing Co.) for 5 min. The resulting average diameters of the particles are ~1–5 μm,[20] ideal for DRIFTS.[19] The NaCl powders were then coated with the unsaturated phospholipid, 1-oleoyl-2-palmitoyl-*sn*-glycero-3-phosphocholine (OPPC) (Sigma Aldrich, 97%). The structure and abbreviations used for the fragments of this molecule throughout this paper are shown in Scheme 1. Coating was accomplished by dissolving 25 mg of OPPC (used as received) in 10 mL of a 9 : 1 (*v*/*v*) mixture of hexane–ethanol, and mixing 1.8 mL of this solution with 1.7 g of NaCl followed by evaporation of the solvent using dry N_2 (Oxygen Service Co., Ultrahigh purity (UHP), > 99.999%). Assuming an area per OPPC molecule of 6×10^{-15} cm^2 per molecule,[21] this is sufficient OPPC to give about a monolayer on cubic salt particles that are 2.0 μm on a side. OPPC/NaCl is used throughout the paper to describe these OPPC-coated powders. It seems likely that OPPC orients itself in a manner similar to that shown in Scheme 1, with the anionic phosphate oxygen and cationic ammonium interacting with the Na^+ and Cl^- ions in the salt, respectively. As discussed below, Auger spectroscopic measurements provide some support for this model of OPPC-coated NaCl.

The morphology and the elemental composition of the OPPC/NaCl was investigated with an FEI/Philips XL-30 Schottky thermal field emission scanning electron microscope coupled to an EDAX energy dispersive X-ray spectrometer (EDS). The SEM and EDS data were collected at a pressure of ~10^{-7} Torr using an accelerating electron beam voltage of 10 kV and magnifications between 5000 and 15500×.

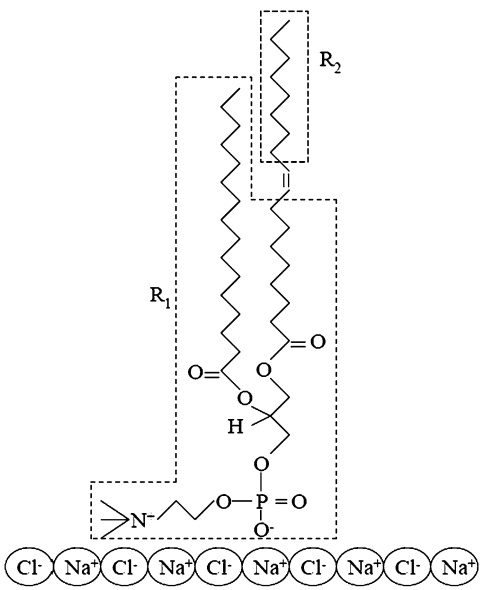

Scheme 1 Model of NaCl crystal coated with of 1-oleoyl-2-palmitoyl-*sn*-glycero-3-phosphocholine (OPPC) used in this study.

DRIFTS cell

The reaction of OPPC/NaCl with ozone was studied in a flow apparatus shown in Fig. 1. A Harrick Scientific diffuse reflection cell (Model DRA-2CS) equipped with a vacuum chamber (Model HVC-DR2) was located in the sample compartment of a Fourier transform infrared spectrometer (Mattson, RS 10000) equipped with a Mattson high-speed transfer board. The reaction chamber consisted of an internal stainless steel sample holder and a stainless steel cover equipped with two symmetrical ZnSe optical windows and a central quartz window. The bottom part of the vacuum chamber was equipped with an internal cooling water system in order to keep the sample at the constant temperature of 296 ± 4 K during each experiment. The internal volume of the assembled vacuum chamber was 11 cm^3. The IR beam entered the first ZnSe window, underwent diffuse reflection in the sample, and was then transmitted through a second ZnSe window to a MCT detector. The total pathlength for the IR beam through the gases in the cell is ~3 cm, which is too small to detect gases in the ppb–ppm range. As a result, the spectra shown here reflect changes in the solid only. Data from 512 scans at 8 cm^{-1} resolution taken over 0.85 min were averaged for one spectrum.

The OPPC/NaCl (350 mg) was placed in the stainless steel holder in the vacuum chamber and compressed[22] in order to form a solid pellet with a geometric surface area of 0.78 cm^2. The sample was pumped for 1 h and then purged with a flow of dry helium (Oxygen Service Co., UHP, >99.995%) for ~30 min. Reactant gases were pumped through the sample at a pumping speed of 1.8×10^{-2} cm^3 s^{-1}.

In some experiments, the reacted mixture was photolyzed using a high pressure Xe arc lamp (Spectra Physics, Oriel 300 W, Model 6258 OF) to probe for photochemically active products. To minimize heating of the sample by the infrared radiation, a 10 cm water filter was placed between the lamp and the DRIFTS cell. A 1 mm Pyrex® glass filter (<10% transmission at $\lambda < 290$ nm) was placed between the UV lamp and the quartz window to remove UV that could photolyze OPPC itself. In separate experiments, OPPC/NaCl was shown to be stable during irradiation with the glass filter in place (but not in its absence). During the photolysis experiments, the temperature of the sample increased by about 5 °C as measured by a thermocouple at the bottom of the salt pellet. After photolysis, it was necessary to let the sample cool for ~30 min in order to return the baseline to its pre-photolysis state.

Ozone was generated by irradiating a dry flow of a He and O_2 mixture with a low-pressure mercury lamp (Jelight company Inc., Double Bore 78-2046). $O(^3P)$ atoms were generated by the dissociation of O_2 (Oxygen Services Co., UHP, >99.993%) and they reacted with O_2 to generate O_3. The O_3 concentration in the mixture was controlled by varying the exposure time of oxygen to the UV light and by adjusting the He dilution. Typical flow rates of 0.4 L min^{-1} were used for He, whereas the flow rates for O_2 ranged between 7 and 55 mL min^{-1} to vary the ozone concentration. Before each experiment, the O_3/O_2/He mixture flowed through the lamp compartment for 1 h to ensure that the ozone concentration was stable.

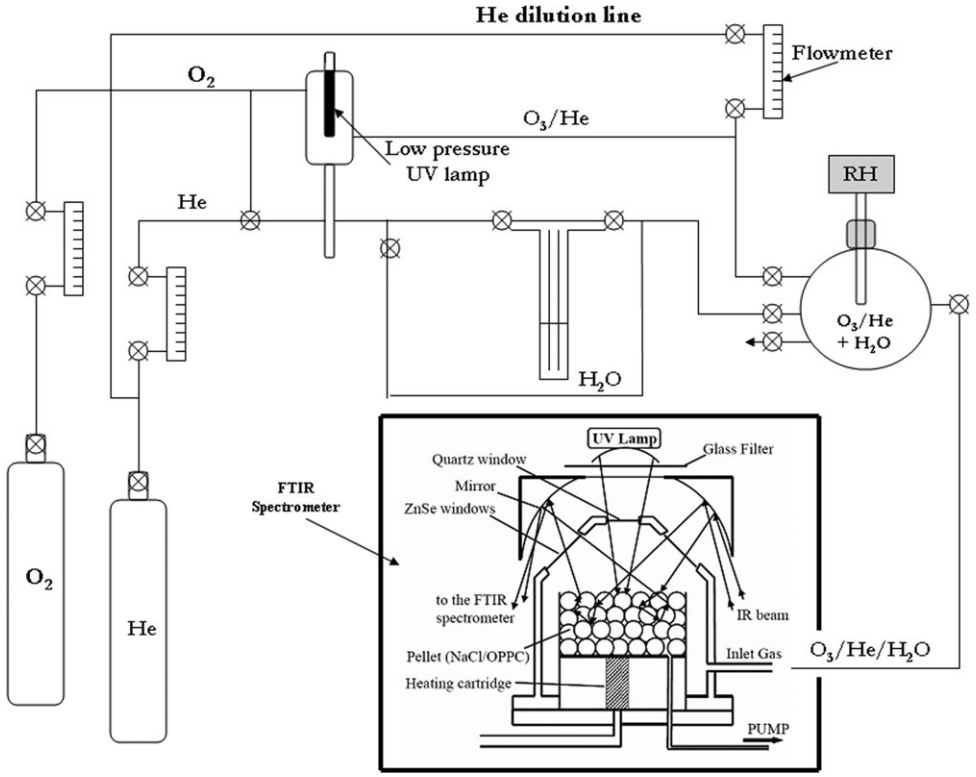

Fig. 1 Schematic diagram of the DRIFTS apparatus and flow system (not to scale).

The O_3/O_2/He mixture was mixed with an additional flow of He in a 5 L darkened bulb at a relative humidity controlled by mixing measured flows of dry and water-saturated He. The water was Nanopure (Barnstead 18 MΩ cm). The O_3 concentration exiting the bulb was measured using an ozone analyzer (Dasibi 1003-AH). The temperature and humidity in the bulb were measured using a sensor (Vaisala HMP234). Since the temperature in the reaction chamber was different than that in the bulb, appropriate corrections were made to determine the relative humidity in the reaction chamber for each experiment.

MALDI-TOF mass spectrometric and Auger spectroscopic analysis

To confirm the products observed by infrared spectroscopy in the DRIFTS experiments, MALDI-MS and Auger spectroscopy were applied to probe OPPC/NaCl before and after ozonolysis. MALDI is a pulsed ionization technique that uses photons to deposit energy rapidly into a mixture of matrix and analyte.[23] Ions are formed through proton or cation (*e.g.*, H^+, Na^+ and K^+) transfer reactions in the expanding gas-phase plume.

The matrix solution for MALDI-TOF experiments was prepared by mixing 20 mg of 2,5-dihydroxybenzoic acid (DHB, Fluka, 99.5% for MALDI-MS) with 40 μL of deionized water and 20 μL of acetonitrile (Sigma Aldrich, LC-MS Chromasolv, 99.9%). The mixture was then microcentrifuged for 30 s to separate undissolved DHB. The OPPC/NaCl samples were prepared by dissolving 20 mg of the salt in 80 μL of water and then adding 80 μL of acetonitrile. About 0.5 μl of this OPPC/NaCl solution was placed on a gold-coated sample plate, and then 0.5 μl of the DHB supernatant solution was added. For the coated samples, the total amount of OPPC was about 80 nmole. The plate was allowed to dry at room temperature, placed in the instrument, and mass spectra were recorded with a Voyager DE STR Biospectrometry Workstation that included a reflectron. The spectrometer was equipped with a nitrogen laser (337 nm, 20 pulses per second, 5 ns width), and a linear detector. An accelerating voltage of 24 700 V was applied for acceleration of ions into the flight tube and a video camera displayed the real-time sample image (80× magnification) on a video monitor.

Auger spectroscopy

The Auger electron spectrometer used was a Physical Electronics model 680 Nanoprobe equipped with a field emission electron source, a cylindrical mirror analyzer and multichannel plate detector. OPPC/NaCl and NaCl crystals were mounted to the sample plate using small pieces of carbon tape. The crystals were analyzed using a 3 nA, 5 kV electron beam using magnifications of 750–1200× such that the entire analysis area was confined to the surface of the salt crystals. Wide scan spectra were obtained to identify the elements present while narrow scan spectra were obtained on carbon KLL, nitrogen KLL, oxygen KLL, sodium KLL, phosphorous LMM, and chlorine LMM for quantification. Quantification was performed on spectra that were subjected to a Savitzky-Golay nine point smoothing and five point derivatization routine. 5 kV sensitivity factors for Na^+ and Cl^- were determined from freshly cleaved NaCl crystals using sputter cleaned Ag as a reference material. All other sensitivity factors were taken from reference tables.[24]

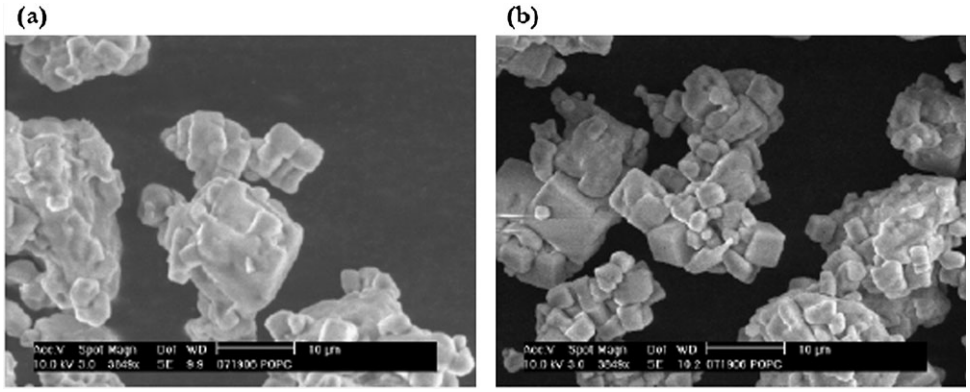

Fig. 2 SEM images of an (a) pure NaCl and (b) NaCl coated with OPPC.

Results and discussion

SEM images of NaCl before and after coating with OPPC are shown in Fig. 2. Coating of the salt by the organic would be expected to result in less water adsorption, including at steps and edges.[25,26] Water is responsible for the rounded appearance of the crystals in Fig. 2a and leads to clumping of the crystallites. Consistent with this, the OPPC/NaCl sample (Fig. 2b) showed a more distinct cubic structure and less agglomeration compared to NaCl, suggesting that the OPPC at least in part coated the salt.

A typical DRIFTS-FTIR spectrum of unreacted OPPC/NaCl is shown in Fig. 3. The spectrum was obtained by taking a ratio of the single beam spectrum of OPPC/NaCl to that of pure NaCl. Assignment of the bands is shown in Table 1.[27–31] Fig. 4 shows spectra for OPPC/NaCl during reaction with 5.0×10^{13} O_3 cm^{-3} at selected times. A new, strong absorption band is formed at $\sim$1110 cm^{-1} that is characteristic of the peroxide C–O bond[32,33] of the secondary ozonide ring (1,2,4-trioxolane, SOZ) known to be formed in ozone–alkene reactions.[14,34–40] New bands at $\sim$1385 and 1347 cm^{-1} are also assigned to the SOZ.[31,33] The peak at 1210 cm^{-1} is assigned to a C–O moiety, although the specific species is not known. New bands appear at 1470 and 2948 cm^{-1}, which track each other as well as the 1110 cm^{-1} SOZ band throughout the experiment. These are at positions expected for C–H bending and stretching modes, respectively, of $-CH_3$ groups. The formation of methyl groups in the ozonolysis of terminal alkene self-assembled monolayers (SAMs) was reported recently, although it is not clear how methyl groups could be formed during oxidation.[41,42] Alternatively, they may be due to C–H stretches associated with the SOZ since the band at $\sim$2948 cm^{-1} is observed upon formation of SOZ and decreases upon its photolysis.

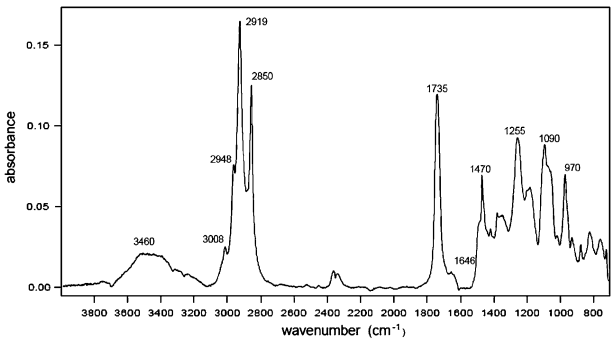

Fig. 3 DRIFTS spectrum of NaCl coated with $\sim$1 monolayer of OPPC (OPPC/NaCl). The spectrum was baseline corrected. The y axis is $\log_{10}(S_1/S_2)$ where S_1 is the single beam spectrum of NaCl alone and S_2 is the single beam spectrum of OPPC/NaCl at RH $\sim$ 0%.

The band at $\sim$1751 cm^{-1} (Fig. 4) is assigned to a non-hydrogen-bonded (free) carboxylic acid.[31] Another carbonyl group is formed at $\sim$1708 cm^{-1}.[28] It is difficult to differentiate between carbonyl absorption due to a hydrogen-bonded carboxylic acid which is red-shifted compared to the free carboxylic acid,[31] and an aldehyde. For example, a peak at $\sim$1710 cm^{-1} was observed for oleic acid on NaCl. However, as discussed below, MALDI spectra show that aldehydes are formed in our experiments. Thus, we assign the 1708 cm^{-1} band to a combination of the aldehyde and hydrogen-bonded carboxylic acids. It is noteworthy that these bands are much smaller in intensity than the SOZ 1110 cm^{-1} band, despite the fact that their absorption coefficients are larger.[31] This establishes that the SOZ is the major product.

The inset to Fig. 4 shows that the formation of products was followed by a decrease in the vinyl C–H stretch at 3008 cm^{-1}, as expected for ozone–alkene reactions. In addition, the $-CH_2-$ antisymmetric (ν_{as}) and symmetric (ν_s) stretches decreased upon reaction with ozone, suggesting a net loss of organic material from the salt mixture. The simultaneous decrease in the intensities of the C–H bands at 3008, 2919 and 2850 cm^{-1} and the increases in the peaks at 1110 cm^{-1} and 1385 cm^{-1} are shown in Fig. 5.

The traditional Criegee mechanism[14,35] for ozone–alkene reactions is shown on the right side of Scheme 2. Modifications to this mechanism, based on the present experimental results, are shown on the left side of Scheme 2. In the scheme and discussion, PL is used to indicate products that retain the choline portion of the reactant phospholipid. Ozone reacts with the double bond to produce a primary ozonide (POZ, 1,2,3-trioxolane) that decomposes to form a C_9 Criegee intermediate (CI) and a PL aldehyde, or a PL Criegee intermediate (PL-CI) and nonanal.[21,34,37,43–45] The fragments can then recombine to form the secondary ozonide. It is noteworthy that the SOZ was stable in this system, and did not show any significant decomposition upon exposure to atmospheric

Table 1 Assignment of the infrared bands observed in the DRIFTS spectra of OPPC/NaCl before and after reaction with O_3, and photolysis

Assignments	Wavenumber/cm^{-1}	Vibrational mode	Ref.
$-N(CH_3)_3^+$	970	N–$(CH_3)_3$ as def.	30, 31
Phosphate	1090	$(PO_2)^-$ sym str	27, 30, 31
SOZ	1110	C–O str	32, 33
Unidentified organic, HCOOH	1210–1220	C–O str	31
Phosphate	1255	$(PO_2)^-$ as str	27, 30, 31
SOZ	1347	C–H def.	33
SOZ	1385	O–C–H bend	33
$-CH_3$	1470	$-CH_3$ bend	31
Carboxylate	1565	CO str	31
H_2O	1646	H–O def.	31
Hydrogen-bonded –COOH, aldehyde	1708	C═O str	31
OPPC ester	1735	C═O str	31, 55
Formate	1730	C═O str	31
Non-hydrogen bonded carboxylic acid –COOH	1751	C═O str	31
Anhydride	1760	C═O str	31, 75
	1820		
RCOCl	1790	C═O str	31
$-CH_2-$	2850	$-CH_2-$ sym str	30, 31
$-CH_2-$	2919	$-CH_2-$ as str	30, 31
$-CH_3$	2948	$-CH_3$ as str	30, 31
C═C	3008	Vinyl C–H str	30, 31
H_2O	3460	H–O str (sym and as)	31

pressure or to water vapor after it had been formed in the reaction.

Additional reaction paths are available for CI's, including isomerization to the acid or reaction with water vapor, if present.[14,43,46–53] The spectrum in Fig. 3 shows that even in the absence of added water vapor, adsorbed water is present on the surface of the OPPC/NaCl. This is a consequence of the charged, zwitterionic polar headgroup on the parent OPPC which strongly attracts and holds water.[54,55] The peak around 3460 cm^{-1} assigned to adsorbed water did not change upon oxidation. Reaction of a CI with water vapor generates either the carboxylic acid or the hydroxyhydroperoxide (HHP) which can decompose to the aldehyde and H_2O_2.[43,46–53]

However, the spectra in Fig. 4 also show that $-CH_2-$ groups are lost during the reaction. This is likely due to the formation of the relatively low molecular weight nonanal (MW = 142) which is pumped away in the gas flow as it is formed. This is consistent with the studies of Wadia *et al.*[45] who measured the formation of gas phase nonanal from the ozonolysis of OPPC on water to be 51 ± 13% (2σ) after correcting for the solubility of nonanal in the water subphase. On the other hand, the PL products and nonanoic acid are expected to remain anchored to the salt. In addition, by analogy to gas-phase ozone–alkene reactions, the CIs may also dissociate and produce OH radicals.[56–63] However, to the best of our knowledge, generation of OH has not been reported for reaction of gas phase ozone with organics on solids.[16,29]

MALDI-TOF analysis

To confirm the identification of the SOZ observed with DRIFTS, OPPC/NaCl was also analyzed after reaction by MALDI-TOF mass spectrometry (Fig. 6). The peak assignments are summarized in Table 2. In addition to adducts of

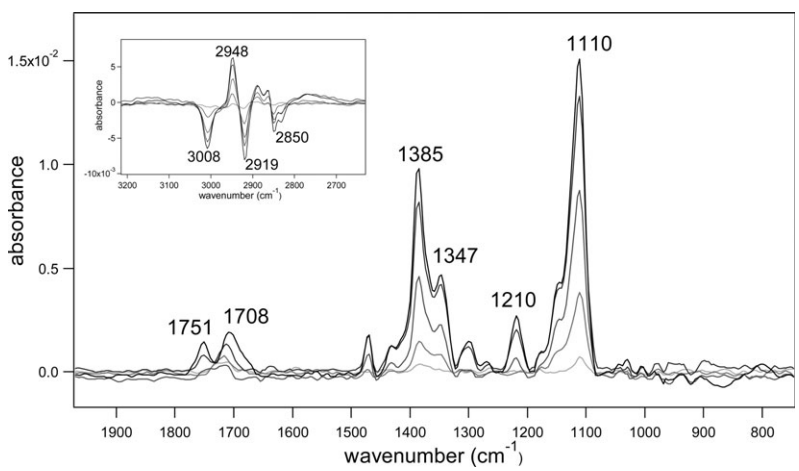

Fig. 4 DRIFTS spectra of OPPC/NaCl upon exposure to 5×10^{13} O_3 cm^{-3} at RH ~ 0%. The y axis is $\log_{10}(S_2/S_3)$ where S_2 is the single beam spectrum of unreacted OPPC/NaCl and S_3 is the single beam spectrum of reacted OPPC/NaCl at increasing ozone exposure times (light gray to black, respectively) of 1, 3, 10, 32 and 56 min.

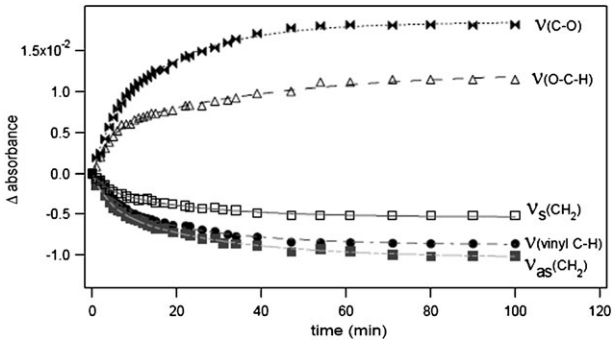

Fig. 5 Changes in absorbance as a function of time for selected bands during reaction of OPPC/NaCl with 5×10^{13} O_3 cm^{-3} at RH $\sim$ 0% (see Table 1). The bands shown are at 1110 cm^{-1} for SOZ ν(C–O) and 1385 cm^{-1} for SOZ (O–C–H), and 3008 cm^{-1} for the vinyl C–H stretch, 2919 cm^{-1} for PL $\nu_{as}(CH_2)$ and 2850 cm^{-1} for PL $\nu_s(CH_2)$.

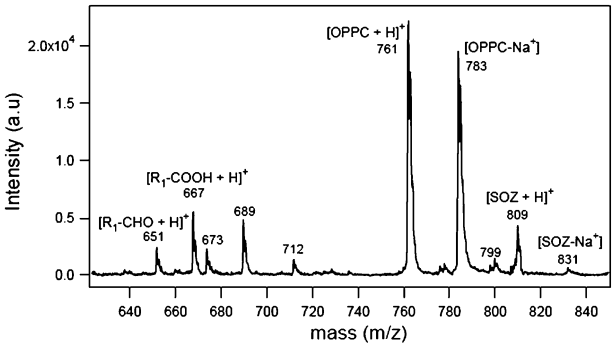

Fig. 6 MALDI-TOF mass spectrum of ozonized sample of OPPC/NaCl with 5×10^{13} O_3 cm^{-3} at RH $\sim$ 0%.

unreacted OPPC, peaks attributable to the SOZ adducts with H^+ and Na^+ are observed at m/z = 809 and 831, respectively. The formation of small amounts of SOZ in the oxidation of unsaturated phospholipids as solids[37] or as a thin film on water[21] was previously reported by Lai *et al.*[37] using fast atom bombardment mass spectrometry.

The protonated ions observed at m/z = 651 and 667 (Fig. 6) are consistent with the molecular ions expected from the PL aldehyde and PL carboxylic acid, respectively (Scheme 2). Alkali metal adduct ions were also observed for PL aldehydes and PL carboxylic acids (see Table 2).

Quantitative measurements of the product yields from the MALDI mass spectra were not possible due to varying signal intensities from the highly variable matrix-to-analyte ratios across the sample.[64–67] However, the MALDI-TOF mass spectra are entirely consistent with the infrared band assignments of the SOZ and PL aldehyde and PL carboxylic acid as products of the ozonolysis of OPPC.

O_3 reaction in the presence of added water vapor

Ozonolysis of OPPC/NaCl was performed in the presence of water vapor at relative humidities (RH) from 2–25%. NaCl crystals deliquesce[68,69] at RH between 72 and 81% and crystallization/effluorescence[68,70] occurs at 42% RH. Experiments in the presence of water vapor were therefore carried out at RH $\leq$25% in order to maintain the integrity of the solid required for DRIFTS. The concentration of ozone was constant at $\sim 5.0 \times 10^{13}$ cm^{-3}.

Fig. 7 shows the spectra obtained when the reaction was carried out at 2, 10 and 25% RH. There is a dramatic decrease in the SOZ band at 1110 cm^{-1} with increasing RH. Bands at 1385 and 1347 cm^{-1} decrease initially but then increase, suggesting that overlapping product bands are growing in simultaneously. For example, the C–H rocking motion in aldehydes occurs in this region.[31] A broad absorption in the 1700–1800 cm^{-1} region with distinct peaks at 1751 and 1708 cm^{-1} increased. As discussed above, the latter were assigned to the non-hydrogen bonded carboxylic acid and to

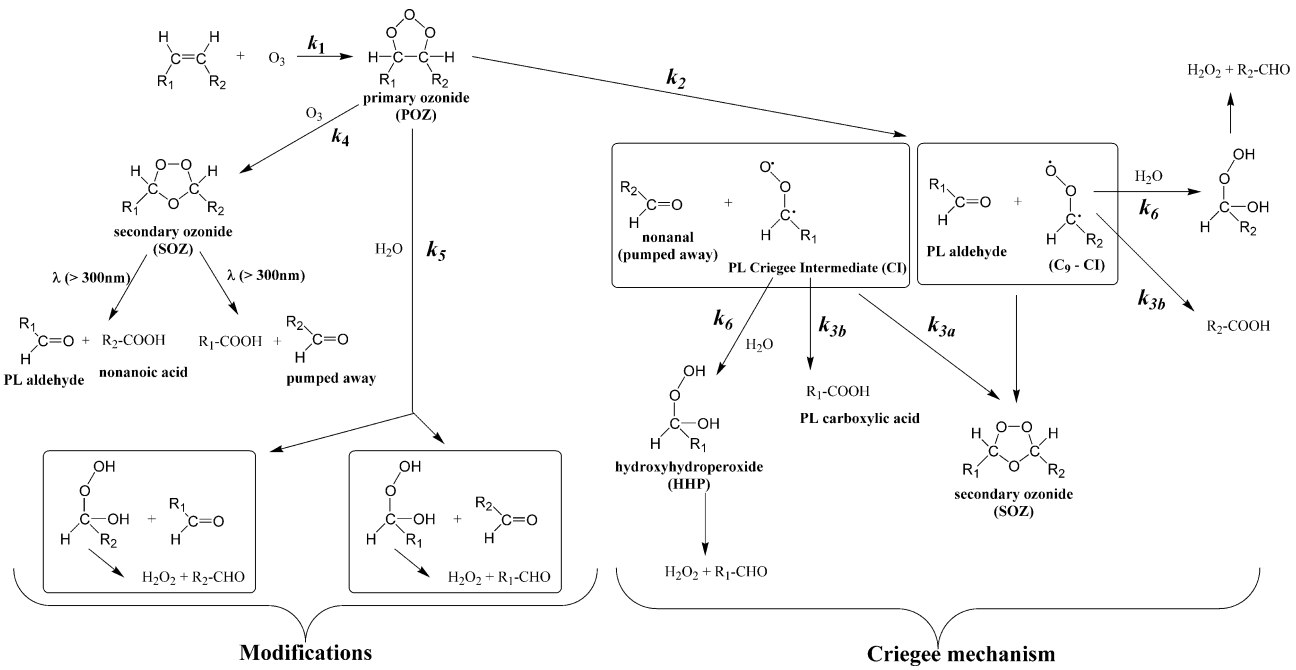

Scheme 2 Summary of heterogeneous ozonolysis of 1-oleoyl-2-palmitoyl-*sn*-glycero-3-phosphocholine (OPPC).

Table 2 MALDI-TOF MS of positive ions obtained from single laser shot of reacted OPPC/NaCl in a matrix of 2,5-dihydroxybenzoic acid (DHB)

Species (adduct)	Molecular mass
SOZ–Na^+ adduct	831
SOZ–H^+ adduct	809
OPPC–K^+ adduct	799
OPPC–Na^+ adduct	783
Unreacted OPPC $[OPPC + H]^+$	761
Carboxylate–$2Na^+$ adduct	712
Carboxylate–Na^+ adduct	689
Aldehyde–Na^+ adduct	673
Carboxylic acid–H^+ adduct	667
Aldehyde–H^+ adduct	651

a combination of the hydrogen-bonded carboxylic acid and PL aldehyde, respectively. In addition, the band at 1210 cm^{-1} assigned to a C–O moiety increased.

Small changes were also observed in the $\nu(PO_2^-)$ antisymmetric and symmetric stretches at ~1261 and ~1090 cm^{-1}, respectively, and at 970 cm^{-1} due to the N–$(CH_3)_3^+$ headgroup.[27] Because the phosphate groups hydrogen bond to water,[54,55] the PO_2^- stretch is extremely sensitive to hydration and hence to the relative humidity. In agreement with previous work of Hübner and Blume,[55] the oxidation experiments showed a shift in the PO_2^- antisymmetric stretching vibration from 1255 to 1261 cm^{-1} when the reaction was carried out in the presence of water vapor. On the other hand, the position of the symmetric PO_2^- band at 1090 cm^{-1} is not sensitive to the presence of water vapor.[55]

Changes in SOZ, aldehydes and carboxylic acids were monitored at an RH of 10% and at O_3 concentrations of 7.0×10^{13} and 1.7×10^{12} cm^{-3}. The relative decrease in SOZ on adding water vapor is more dramatic at the lower ozone concentration, suggesting that the CI which forms the SOZ can also react with water vapor in competition with SOZ formation. This is consistent with the chemistry in Scheme 2. However, even at 10% RH, the water vapor concentration is large (7.0×10^{16} cm^{-3}) so that this reaction competes with other fates of the CI. In aqueous solution, the rate of reaction of CI with water has been shown to be faster than its reaction with aldehydes to form the SOZ.[43]

As discussed earlier, the reaction with water is known to form carboxylic acids as well as hydroxyhydroperoxides (HHP) which in the gas phase can decompose to the corresponding aldehyde and H_2O_2, to the acid and water, or to OH and organic free radicals.[71] Formation of HHPs has been observed previously[43,46,48–53] and direct evidence for their formation in phospholipid ozonolysis was obtained using ^{13}C NMR.[49]

The increase in the aldehyde and carboxylic acid peaks on addition of water vapor is consistent with these reactions. It should be noted that in separate experiments, addition of water after the reaction had ceased did not change the SOZ peak, showing that it is not the SOZ itself that reacts with water vapor.

Photolysis

Fig. 8 (black line) shows the DRIFTS spectrum of reacted OPPC/NaCl after 135 min of UV photolysis at $\lambda \geq 300$ nm compared to the spectrum before photolysis but after reaction with 5.0×10^{13} cm^{-3} of ozone for ~100 min (gray line). OPPC does not absorb light and photolyse at $\lambda \geq 300$ nm, which was confirmed in separate experiments. However, as seen in Fig. 8, the bands assigned to SOZ at ~1110, 1385, and 2948 cm^{-1} decreased upon exposure to the UV light, which is not surprising because the peroxide O–O bond is very weak.[14] Bands in the 2850–2950 cm^{-1} and 1470 cm^{-1} regions associated with C–H also decreased, suggesting the formation of more volatile products which are pumped away.

There were also significant changes in the carbonyl region. As shown in Fig. 8b, the spectrum after photolysis could be fitted by six overlapping peaks at 1820, 1790, 1760, 1751, 1730, and 1708 cm^{-1}. The new bands at ~1730 and 1210 cm^{-1} were assigned to surface adsorbed HCOOH based on reference experiments in which similar bands typical of this acid[31] were observed when NaCl was exposed to gaseous HCOOH. Recent studies by Nizkorodov and coworkers on the ozonolysis of SAMs, undecylenic acid films and d-limonene reported formation of formaldehyde (HCHO) and formic acid (HCOOH) as gas-phase products upon photolysis of the ozonized organic ($\lambda > 295$ nm).[72–74] The major source of

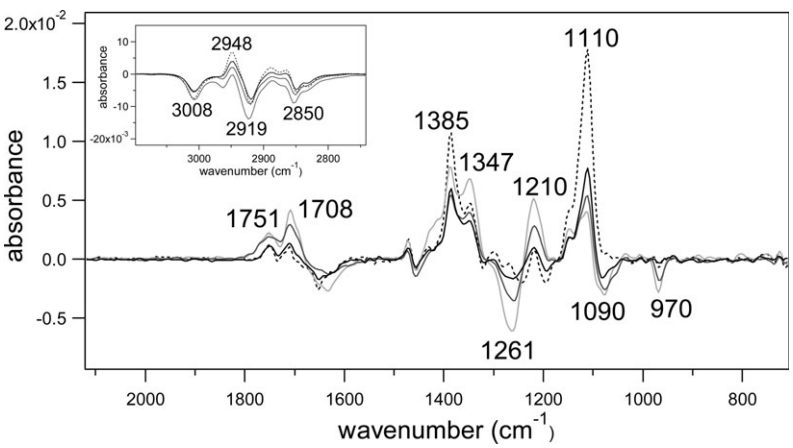

Fig. 7 DRIFTS spectra of OPPC/NaCl upon exposure to 5×10^{13} O_3 cm^{-3} in the presence of water vapor. The y axis is $\log_{10}(S_2/S_3)$ where S_2 is the single beam spectrum of unreacted OPPC/NaCl and S_3 is the single beam spectrum of reacted OPPC/NaCl at relative humidities of 2, 10 and 25% RH (black to light gray, respectively). The dashed line is the DRIFTS spectrum for a sample reacted with ozone at RH ~ 0.

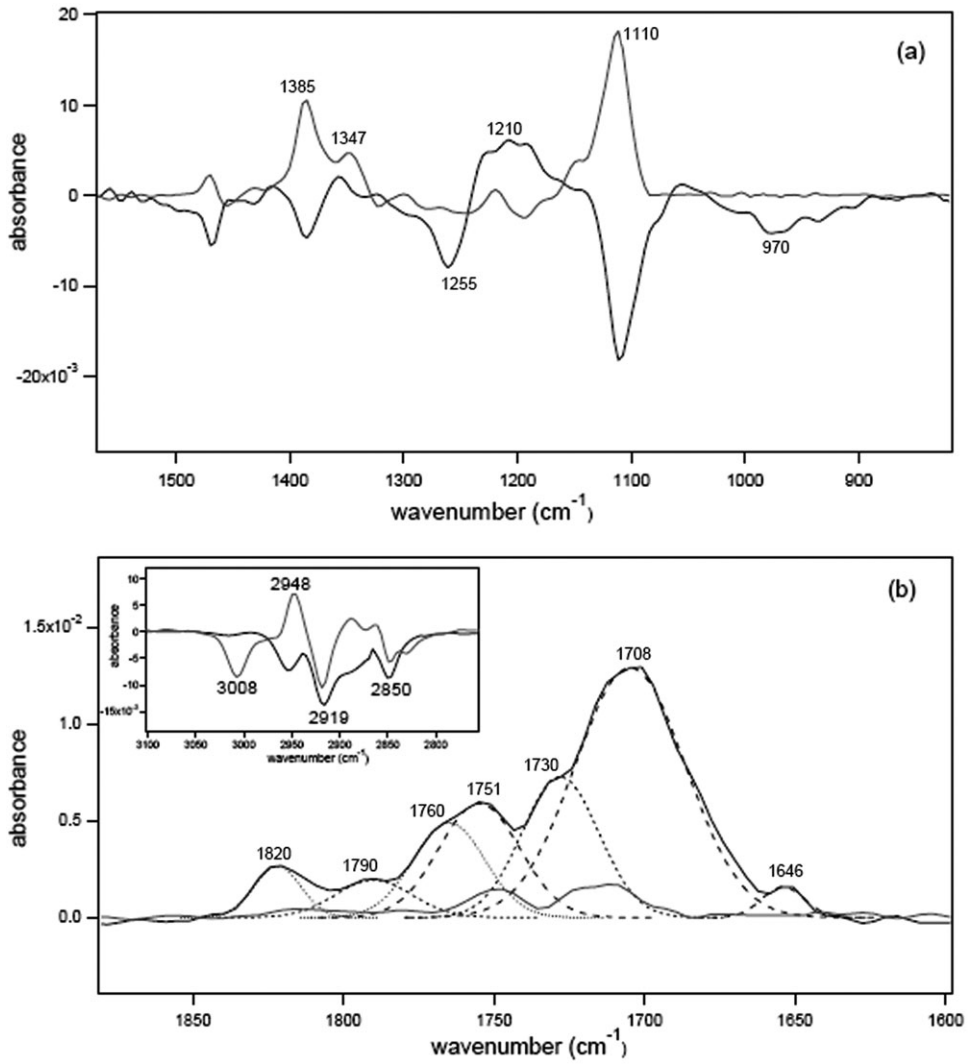

Fig. 8 DRIFTS spectra from OPPC/NaCl reacted with 5×10^{13} O_3 cm^{-3} and then photolyzed. The black line is $\log_{10}(S_3/S_4)$ where S_3 is the single beam spectrum of oxidized OPPC/NaCl and S_4 is the single beam spectrum of oxidized OPPC/NaCl after photolysis. The gray line is $\log_{10}(S_2/S_3)$ where S_2 is the single beam spectrum of unreacted OPPC/NaCl. (a) The spectra are shown in the 800–1600 cm^{-1} region and (b) in the C═O and C–H stretching regions. The dotted and dashed lines in (b) represent the components obtained from the fit of the broad band in the 1650–1850 cm^{-1} region.

these products was attributed to scission of the weak O–O bond to generate intermediates which decomposed to gaseous formic acid or formaldehyde together with surface aldehyde and carboxylic acid. The observation of adsorbed HCOOH in the present studies suggests that it is also formed in the photolysis of the OPPC ozonide.

The C═O stretching vibrations at 1760 and 1820 cm^{-1} were assigned to an anhydride.[31] It is interesting that similar bands were reported in the ozonolysis of an alkene thiol self-assembled monolayer (SAM) on gold in the dark.[75] Combined with the significant SOZ loss, these data suggest that the SOZ photolyzes to form the anhydride, at least in part. This is in agreement with the work of Story[76] who reported the formation of anhydrides in the photolysis of SOZ in solution. He proposed cleavage of the weak O–O bond followed by a double β-scission to eliminate alkyl groups which combined to form stable hydrocarbon products. In the present experiments, some of the hydrocarbon products formed would be removed by pumping, which may be responsible for simultaneous decrease in the CH bands in the 2900 cm^{-1} region (Fig. 8b). Alternatively, if photolysis gives more carboxylic acids and these are sufficiently closely packed to interact, they could dehydrate to form the anhydride. The spectra in Fig. 8 show that there is indeed an increase in the bands at 1751 and 1708 cm^{-1} due to carboxylic acids during photolysis. The peak at 1790 cm^{-1} is assigned to an acid chloride, RCOCl,[31] which would be expected if free radical reactions were induced by photolysis.

To further probe for the presence of carboxylic acid (–COOH), the oxidized and photolyzed OPPC/NaCl sample was exposed to gaseous NH_3/H_2O from the vapor over an aqueous ammonia solution. Ammonia reacts with carboxylic acids to form ammonium carboxylate salts. Fig. 9 shows that the major peaks at 1708, 1751 and 1820 cm^{-1} decrease on exposure to NH_3/H_2O, while a strong peak appears at 1565 cm^{-1}. The latter is assigned to carboxylate which has a

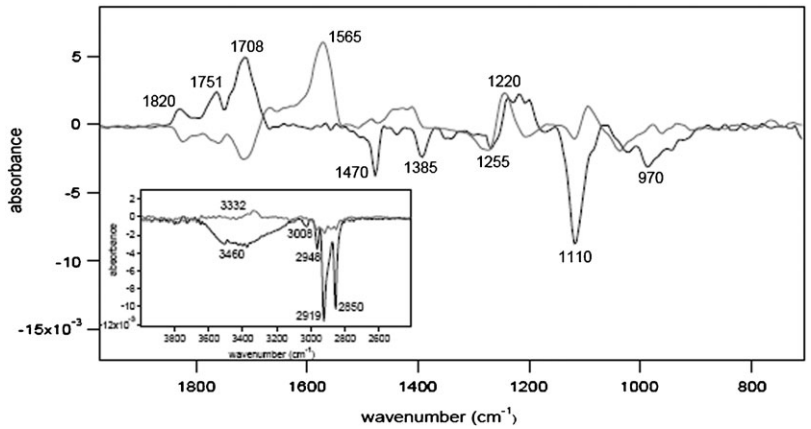

Fig. 9 Changes in the DRIFTS spectrum of an OPPC/NaCl sample that had been reacted with 5×10^{13} O_3 cm^{-3}, photolyzed and then reacted with NH_3/H_2O. The black line is $\log_{10}(S_3/S_4)$ where S_3 is the single beam spectrum of oxidized OPPC/NaCl and S_4 is the single beam spectrum of oxidized OPPC/NaCl after photolysis. The gray line represents $\log_{10}(S_4/S_5)$ where S_5 is the single beam spectrum of oxidized OPPC/NaCl after photolysis and reaction with NH_3/H_2O.

vibration[31] in the region of 1585–1560 cm^{-1}. Weaker overlapping peaks in the 1400 cm^{-1} region are also formed which are assigned to carboxylate.[31] The decrease in the 1751 and 1708 cm^{-1} peaks is expected if they are due to carboxylic acids. The decrease in the 1820 cm^{-1} peak suggests that the anhydride is hydrolyzing to the carboxylic acid which reacts with NH_3 to form R–COO^-. As seen in the inset to Fig. 9, a band at 3332 cm^{-1} due to NH_4^+ is also observed.

In separate experiments, small amounts of carboxylate formation were observed from the reaction of gaseous NH_3/H_2O with unreacted OPPC/NaCl. This may be due to some hydrolysis of the reactant ester groups followed by their reaction with NH_3. However, the intensity of the band at 1565 cm^{-1} was considerably larger for the reaction of gaseous NH_3 with an oxidized and photolyzed OPPC/NaCl sample.

Auger spectroscopic analysis

Analysis by Auger spectroscopy was performed on samples of NaCl with and without the OPPC coating as well as on coated samples after reaction with ozone and UV photolysis. Table 3 summarizes the elemental composition of the samples.

As expected, NaCl has, within experimental error, a 1 : 1 Na : Cl ratio. Small amounts of C and O were present in the NaCl as contaminants, but the OPPC/NaCl sample shows much larger amounts of C and O. However, the increase in O was much less than the amount expected from the formula of OPPC, which has an O : C ratio of 1 : 5. In addition, while both the Na and Cl signals were attenuated, the signal due to Cl was much more strongly affected by the coating. Interestingly, neither P nor N were detected above the background level.

Table 3 Elemental composition obtained by Auger spectroscopy of OPPC/NaCl samples

Sample	[a]Atomic concentration (%)					
	Na	Cl	C	O	P	N
NaCl	46	51	2.4	1.2		
OPPC/NaCl	34	8.6	54	3.9	<0.1	
OPPC/NaCl + O_3 [b]	41	14	39	6.3	<0.1	<0.4
(OPPC/NaCl + O_3) + UV[c]	36	11	49	3.2	<0.1	<0.5

[a] Auger spectra related to these data were obtained in multiplex mode (narrow scan). Analysis of different particles give errors of ±2% on Na and ±4% on Cl. [b] $O_3 = 5.0 \times 10^{13}$ molecule cm^{-3}. [c] Same as (b) but with 135 min photolysis with $\lambda > 300$ nm.

Several factors come into play in determining the relative signal intensities for this type of coated sample. Auger electrons have a certain escape depth due to their collisions with other atoms on their way towards the surface. Hence, their kinetic energy decays exponentially with distance from the surface. If these electrons are from atoms that are sufficiently deep (distances greater than their inelastic mean free path), they can lose enough energy to contribute only to the background signal. This will be particularly true for Auger electrons with low kinetic energy.[77] The small oxygen signal in the coated sample may be due to the fact that the oxygen is next to the NaCl surface, buried under the long carbon chains which project into the vacuum. The greater attenuation of the chlorine signal compared to the sodium is due to the smaller kinetic energy of the chlorine atom Auger electrons, 185 eV compared to 996 eV for Na. Similar factors are likely responsible for the lack of detection of phosphorus and nitrogen which have 123 and 380 eV Auger electrons, respectively.

The ozonized OPPC/NaCl had relatively more O and less C, as qualitatively expected based on the products of the reaction identified using DRIFTS and MALDI-TOF MS. If the OPPC is completely converted to the SOZ, then the O : C ratio should increase by 38% compared to the unreacted sample. The data in Table 3, however, show that this ratio actually more than doubles. This is likely due to the fact that the oxygen in the products is not buried under long organic chains, and hence the signal is not attenuated as much as for the unreacted OPPC/NaCl. In addition, DRIFTS clearly showed a net loss of C–H groups during the reaction, which was attributed to the formation and removal of volatile products such as nonanal, HCHO and HCOOH. Thus a net loss of carbon is expected, which will also increase the O : C ratio. Finally, reaction is expected to lead to scission of the long chains, decreasing the film thickness. This is also consistent with

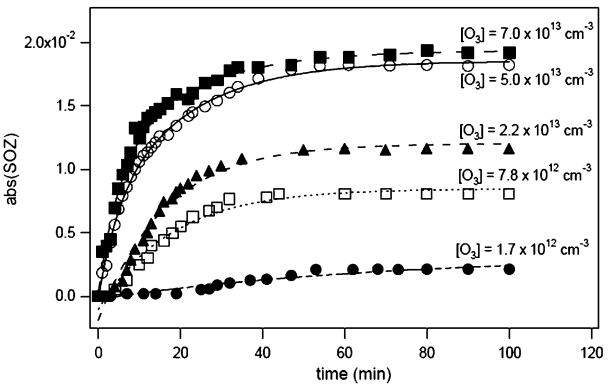

Fig. 10 Changes in absorbance of the SOZ (–C–O–) band at 1110 cm^{-1} as a function of exposure time and ozone concentration.

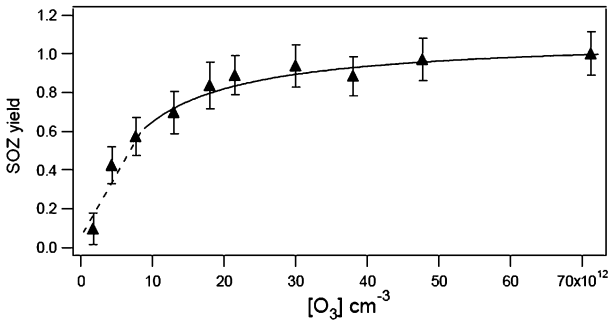

Fig. 11 Plot of the SOZ yield ([SOZ]/Δ[OPPC]) *versus* [O_3] at t = 100 min.

increased signals due to the underlying salt after reaction. After photolysis, the elemental composition measured using Auger spectroscopy is similar to that of unreacted OPPC/NaCl. This suggests that during photolysis, volatile products containing oxygen are generated.

Kinetics

DRIFTS measurements are very useful for following reactions on surfaces in real time, which allows rate constants to be determined.[20] As shown in Fig. 10, the ozonolysis of OPPC/NaCl was monitored by measuring the change in the absorbance (Δ absorbance) of the SOZ 1110 cm^{-1} band as a function of time. The intensity of the absorbance is linearly related to the secondary ozonide surface coverage,[20]

$$\frac{\text{abs(SOZ)}_t}{\text{abs(SOZ)}_\infty} = \frac{[\text{SOZ}]_t}{[\text{SOZ}]_\infty} \qquad \text{(I)}$$

where abs(SOZ) and $[SOZ]_t$ represent the absorbance of the 1110 cm^{-1} band and the total surface concentration of secondary ozonides at time t, respectively, $t = \infty$ represents the time at which there is no further formation of products. While other products are clearly formed (Fig. 4), the large intensity of the SOZ peaks relative to the carbonyls suggests that SOZ is the major product at high O_3 concentrations and we assume for these calculations that the SOZ yield is 100% under these conditions, *i.e.*, one SOZ is formed initially for each OPPC reacted. If all of the OPPC is oxidized, $[SOZ]_\infty$ is expected to be equal to the initial surface density of the original monolayer (1.6×10^{14} OPPC cm^{-2}),[21] and this should be the same for different ozone concentrations.

Fig. 10 shows the increase in the absorbance at 1110 cm^{-1} due to the SOZ as a function of time for five different O_3 concentrations but the same initial amount of OPPC. Unexpectedly, the final amount of SOZ increases with the ozone concentration. However, at the higher O_3 concentrations, it is converging to a common value at long reaction times.

Based on the change in the intensity of the 3008 cm^{-1} band, only about 20% of the initial OPPC reacted at all ozone concentrations, suggesting that not all of the OPPC in the sample is actually available for reaction. This could be due to some of the OPPC being in aggregates where only the double bonds on the surface are available for reaction, or that the unreacted double bonds become shielded by structural changes that occur as the oxidation proceeds. In either case, it is assumed that the initial OPPC actually available for reaction is 20% of that in the sample, or 3.2×10^{13} OPPC cm^{-2} (Δ[OPPC]), and that this is the limiting amount of SOZ that can be formed at the plateau (Fig. 10) at $[O_3] = 7 \times 10^{13}$ cm^{-3}. The absorbance of the SOZ at this plateau was then used to obtain the concentrations of SOZ as a function of time and ozone concentration by scaling the measured absorbances to this value. From the concentration of SOZ and loss of OPPC, the yield of SOZ at the plateau was calculated. Fig. 11 shows a plot of the SOZ yield as a function of [O_3]. It is clear that not only the rate of formation of the SOZ (Fig. 10), but also its final yield (Fig. 11) increased with O_3, tending to asymptotic values at the higher concentrations.

From eqn (I), the rate of formation of SOZ is given by the following expression:

$$\left(\frac{\text{d}[\text{SOZ}]}{\text{d}t}\right)_t = \left(\frac{\text{d}[\text{abs(SOZ)}]}{\text{d}t}\right)_t \times \frac{[\text{SOZ}]_\infty}{\text{abs(SOZ)}_\infty} \qquad \text{(II)}$$

The rate of change of the absorbance at ~1110 cm^{-1}, d[abs(SOZ)/dt], was calculated from the derivative of the best fit to the experimental absorbance data (Fig. 10), abs(SOZ)_∞ from the plateau at long reaction times, and the corresponding $[SOZ]_\infty$ as described above. Fig. 12 shows a plot of the rate of formation of the SOZ extrapolated to $t = 0$ for each experiment as a function of the initial ozone concentration.

The conventional Criegee mechanism (Scheme 2) for the formation of SOZ involves the formation of a primary ozonide (POZ),

$$\text{O}_3 + \text{OPPC} \xrightarrow{k_1} \text{POZ} \qquad (1)$$

followed by its decomposition to CIs and aldehydes that recombine to form SOZ:

$$\text{POZ} \xrightarrow{k_2} \text{CI} + \text{RCHO} \qquad (2)$$

$$\text{CI} + \text{RCHO} \xrightarrow{k_{3a}} \text{SOZ} \qquad (3a)$$

$$\text{CI} \xrightarrow{k_{3b}} \text{products} \qquad (3b)$$

Decomposition of CIs yields products which may include carboxylic acids. This reaction mechanism is somewhat

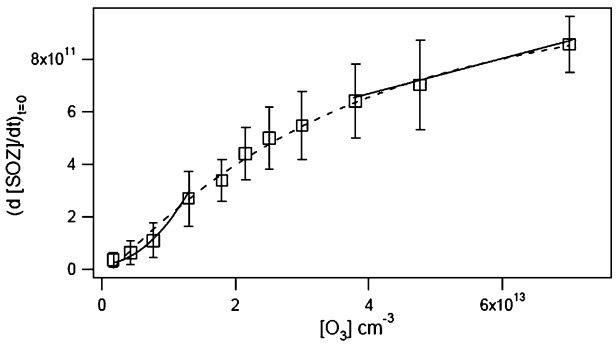

Fig. 12 Initial rate of formation of SOZ (molecules cm^{-2} s^{-1}) as a function of gas-phase ozone concentration. Solid lines are the fits based on eqn (V) in the approximation of high and low ozone concentrations. Dashed lines represent the whole set of data points fitted with eqn (V).

simplified, of course, and as written, assumes that the species are adsorbed on the surface. While nonanal is expected to desorb at least partially during pumping, it has opportunities to react further while passing through the salt. It is not expected that this will alter the kinetic analysis significantly.

If reactions (2), (3a) and (3b) are fast relative to reaction (1), the rate of formation of the SOZ should depend linearly on the O_3 concentration. However, Fig. 12 shows a more complex dependence of the initial rate of SOZ formation on O_3, increasing rapidly with concentration at low $[O_3]$, and then becoming linear at high concentrations. In addition, the SOZ yield increases with the concentration of O_3 (Fig. 11). These observations suggest that there are additional mechanisms of SOZ formation than represented by reactions (1)–(3b). We propose that this involves the reaction of POZ with O_3 to generate SOZ, and that this reaction dominates SOZ formation under most of our experimental conditions. In the following, it is demonstrated that such a mechanism is consistent with the measured reaction kinetics.

The modified mechanism we propose consists of reactions (1)–(3b) and reaction (4):

$$O_3 + POZ \xrightarrow{k_4} SOZ \qquad (4)$$

The steady state concentration of POZ at the surface is given by eqn (III)

$$[POZ]_{SS} = \frac{k_1[O_3][OPPC]}{k_2 + k_4[O_3]} \qquad (III)$$

and that of the Criegee intermediate by eqn (IV):

$$[CI]_{ss} = \frac{k_2[POZ]_{SS}}{\{k_{3a}[RCHO] + k_{3b}\}} = \frac{k_1 k_2[O_3][OPPC]}{\{k_{3a}[RCHO] + k_{3b}\}\{k_2 + k_4[O_3]\}} \qquad (IV)$$

The initial rate of change of [SOZ] is given by the following expression:

$$\left(\frac{d[SOZ]}{dt}\right)_{t=0} = k_{3a}[CI]_{ss}[RCHO] + k_4[O_3][POZ]_{ss} = \frac{k_1[OPPC][O_3]}{(k_2 + k_4[O_3])}\left[\frac{k_2 k_{3a}[RCHO]}{(k_{3a}[RCHO] + k_{3b})} + k_4[O_3]\right] \qquad (V)$$

At high ozone concentrations ($\geq 4 \times 10^{13}$ cm^{-3}), the initial rate of formation of [SOZ] approaches $k_1[O_3][OPPC]$ and hence is linear in $[O_3]$. From the measured rate of SOZ formation and initial reactant concentrations, a value was calculated for $k_1 = (4.5 \pm 0.6) \times 10^{-16}$ cm^3 $molecule^{-1}$ s^{-1} (2σ).

The ozonolysis of OPPC as a surfactant layer on water was studied by Lai *et al.*[21] who followed the loss of OPPC from the surface, and by Wadia *et al.*[45] who measured the formation of gas phase nonanal. These metrics both gave a lower limit for the reaction probability, γ, for O_3 reacting with OPPC of $\geq 3 \times 10^{-6}$. Because the mechanism we propose here is more complex than reaction during one collision, the use of reaction probabilities is not strictly correct. However, if we convert our current value of k_1 at 1 ppm O_3 (within the range covered by the previous studies) to an effective reaction probability, we obtain $\gamma = 8 \times 10^{-6}$, consistent with the lower limit reported earlier. By analogy to gas phase ozone–alkene reactions where room temperature rate constants for internal alkenes correspond to reaction probabilities of $\sim 10^{-7}$, it is again clear that the reaction kinetics on solids are greatly enhanced. As discussed in detail by Tobias and coworkers,[78] this is due to trapping of ozone in the organic film, which increases the number of ozone-double bond collisions and hence the opportunity for reaction.

The term $k_2k_{3a}[RCHO]/(k_{3a}[RHCO] + k_{3b})$ in (V) is equivalent to $k_2\phi$, where ϕ is the branching ratio for the removal of the CI by reaction with RHCO. If this term is small compared to $k_4[O_3]$ under our experimental conditions, then at low O_3 concentrations (approaching $\sim 10^{12}$ cm^{-3}) the initial rate of formation of SOZ approaches k_1k_4 $[O_3]^2[OPPC]/k_2$. The data in Fig. 12 at low O_3 concentrations were well fit with such a function in $[O_3]$. Using the value of k_1 of $(4.5 \pm 0.6) \times 10^{-16}$ cm^3 $molecule^{-1}$ s^{-1}, a value for the ratio of the rate constants $k_4/k_2 = (1.1 \pm 0.5) \times 10^{-13}$ cm^3 $molecule^{-1}$ (2σ) was derived.

The experimental data in Fig. 12 were fit to the form of eqn (V) by taking $k_1 = (4.5 \pm 1.2) \times 10^{-16}$ cm^3 $molecule^{-1}$ s^{-1}, $k_4/k_2 = (1.1 \pm 0.5) \times 10^{-13}$ cm^3 $molecule^{-1}$ but allowing k_4 and k_2 to vary freely. This curve fitting gave $k_4 = (1.1 \pm 0.6) \times 10^{-12}$ cm^3 $molecule^{-1}$ s^{-1} and $k_2 = (10 \pm 2.0)$ s^{-1}. It should be noted that these errors are statistical only, which for k_1 and the ratio k_4/k_2, is adequate. However, since values for k_4 and k_2 could not be derived independently, the uncertainty in these rate constants will be greater.

This analysis at small concentrations of O_3 assumes that the term $k_2\phi$ is small compared to $k_4[O_3]$. At the smallest concentration of O_3 used, 1.7×10^{12} cm^{-3}, these terms are equal for a branching ratio for reaction (3) of $\phi = 0.2$. At smaller values of the branching ratio and/or higher ozone concentrations, this assumption is clearly reasonable.

The lifetime of the POZ with respect to thermal decomposition is given by $\tau_{POZ} = 1/k_2 \sim 100$ ms. This can be compared to the studies of Mile *et al.*[79] who measured the kinetics of decomposition of a number of primary ozonides in solution at low temperatures. For decomposition of the POZs of *cis*-di-isopropylethylene, and of 1-hexene for example, the pre-exponential factors were estimated to be 10^3 s^{-1} and the activation energies less than 14 kJ mol^{-1}. With the latter value for E_a, the rate constant at 298 K is 3.5 s^{-1}, giving a lifetime of 300 ms. A rate constant for decomposition and lifetime equal to 100 ms would be obtained for an activation energy of 11 kJ mol^{-1}.

In order for reactions (1)–(4) to represent the mechanism, the lifetime of the POZ must be sufficiently long to allow for reaction with O_3. At an ozone concentration of 7.5×10^{12} molecules cm^{-3}, the number of collisions of O_3 per cm^2 of salt per second is 6.8×10^{16}, assuming there is no diffusion limitation. Since the average coverage of OPPC on the salt is 1.6×10^{14} OPPC cm^{-2}, the time for an OPPC-O_3 collision is of the order of 2 ms. Of course, not every ozone collision will lead to reaction. However, this comparison suggests that it is reasonable that the POZ has a sufficiently long lifetime to react with O_3, and that the POZ-O_3 reaction will become increasingly important as the O_3 concentration increases.

To the best of our knowledge, reaction of a POZ on a solid with gases has not been reported before. However, Jung and Davidov[80] did report trapping of a primary ozonide in the ozonolysis of bicyclic allylic alcohols in solution at 25 °C.

With water vapor addition

In the presence of water vapor, the formation of the SOZ is decreased (Fig. 7). Although CI's are known to react with water which would decrease the SOZ formation *via* reaction (3a), the kinetics and stoichiometry discussed above establish that it is the POZ reaction with O_3 that is the major source of SOZ in this system at the higher O_3 concentrations. The decrease in the SOZ with water vapor suggests that the POZ also reacts with water vapor. As a result, reactions of both the POZ and the CI with water were added to the reaction scheme:

$$H_2O + POZ \xrightarrow{k_5} \text{products} \quad (5)$$

$$H_2O + CI \xrightarrow{k_6} \text{products} \quad (6)$$

For oxidation experiments performed at different relative humidities, the steady state concentration of POZ at the surface is then given by eqn (VI),

$$[POZ]_{SS} = \frac{k_1[O_3][OPPC]}{k_2 + k_4[O_3] + k_5[H_2O]} \quad (VI)$$

and that of the CI by eqn (VII):

$$[CI] = \frac{k_2[POZ]_{SS}}{k_{3a}[RCHO] + k_{3b} + k_6[H_2O]} = \frac{k_1k_2[OPPC][O_3]}{\{k_{3a}[RCHO] + k_{3b} + k_6[H_2O]\}\{k_2 + k_4[O_3] + k_5[H_2O]\}} \quad (VII)$$

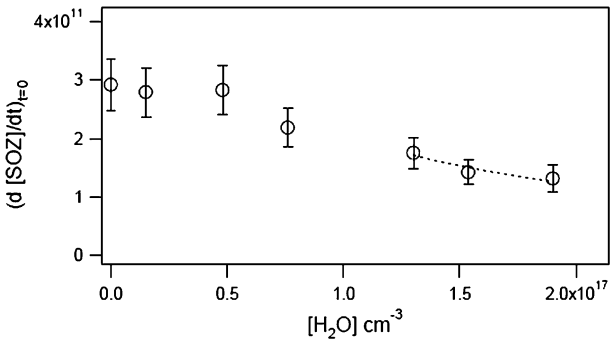

Fig. 13 Initial rate of formation of SOZ as a function of water vapor concentration. Solid line is the fits based on eqn (VIII) in the approximation of high water vapor concentrations at 5×10^{13} O_3 cm^{-3}. Dashed line is the partial fit of all the data points to eqn (VIII).

The initial rate of change of [SOZ] at $t = 0$ is then given by eqn (VIII):

$$\left(\frac{d[SOZ]}{dt}\right)_{t=0} = \frac{k_1k_2k_{3a}[RCHO][O_3][OPPC]}{\{k_2 + k_4[O_3] + k_5[H_2O]\}\{k_{3a}[RCHO] + k_{3b} + k_6[H_2O]\}} + \frac{k_1k_4[O_3]^2[OPPC]}{k_2 + k_4[O_3] + k_5[H_2O]} \quad (VIII)$$

At small water vapor concentrations ($\leq 10^{16}$ cm^{-3}), reactions (5) and (6) are not competitive with other reactions of the POZ and CI and the rate should be independent of water vapor. At high water vapor concentrations ($\geq 10^{17}$ cm^{-3}), the rate should vary with the inverse of the water vapor concentration if the POZ is the major SOZ source. If the CI reactions (3a) and (3b) also contribute significantly, then the rate of SOZ formation will decrease with increasing water concentrations, but in a more complex manner.

Fig. 13 shows a plot of the initial rate of formation of [SOZ] as a function of water vapor concentration at a constant ozone concentration of 5×10^{13} molecule cm^{-3}. As predicted by eqn (VIII), the rate does not vary with the water vapor concentration at low concentrations, but does vary inversely with H_2O at high concentrations. Using the previous calculated values of k_1 and k_4 it was possible to fit the data at high water vapor concentrations in Fig. 13 (dashed line) and estimate values for k_5 of $(1.3 \pm 0.5) \times 10^{-15}$ cm^3 $molecule^{-1}$ s^{-1} and for k_6 of $(1.0 \pm 0.3) \times 10^{-17}$ cm^3 $molecule^{-1}$ s^{-1}. The latter value is similar to that estimated for analogous gas phase reactions of the CI with water.[14,47]

Conclusions and atmospheric implications

These experiments show that the ozone–alkene chemistry on solids is quite different from that in the gas phase or in solution. In particular, the primary ozonide formed on addition of O_3 to the double bond is sufficiently stable, with a lifetime of ~100 ms, that it can undergo further reactions with O_3 and with water vapor. Although other gases such as SO_2

Table 4 Summary of kinetics for the O_3-OPPC system

Reaction	Rate constant[a]	[X][b]	τ[c]
O_3 + OPPC	$(4.5 \pm 0.6) \times 10^{-16}$	100 ppb	15 min
POZ + O_3	$(1.1 \pm 0.6) \times 10^{-12}$	100 ppb	370 ms
POZ → CI + RHCO	10 ± 2		100 ms
POZ + H_2O	$(1.3 \pm 0.5) \times 10^{-15}$	3.8×10^{17} (50% RH)	2 ms
CI + H_2O	$(1.0 \pm 0.3) \times 10^{-17}$	3.8×10^{17} (50% RH)	260 ms

[a] Rate constants in units of cm^3 $molecule^{-1}$ s^{-1} except for the POZ decomposition which has units of s^{-1}; cited errors are statistical (see text). [b] Concentrations of O_3 or H_2O assumed for lifetime τ estimates. [c] Calculated lifetime of OPPC, POZ or CI, respectively.

were not studied in these experiments, it seems likely that they would also be oxidized by the POZ.

Table 4 summarizes the kinetics data from these studies, as well as lifetimes for OPPC, the POZ and the CI at an O_3 concentration of 100 ppb and a water vapor concentration corresponding to 50% RH at 298 K. The ozone reaction with OPPC is sufficiently fast that a lifetime of only 15 min is expected in the atmosphere at 100 ppb O_3. Even at typical concentrations of O_3 in remote regions, the OPPC lifetime will still be only of the order of an hour.

It is clear from the data in Table 4 that the reaction with H_2O will under most circumstances be the major removal path for the POZ in the atmosphere. Although the products of this reaction are not known, they may be similar to those of the CI, *i.e.*, acids, hydroxyhydroperoxides and the aldehyde. However, the direct conversion of the POZ will be somewhat faster than decomposition to the CI followed by its reaction with water.

There may be situations where formation of the SOZ represents a significant part of the reaction. For example, consider polluted, dry areas such as Mexico City[81,82] with O_3 peaks of ~400 ppb. Under dry conditions with RH ~20%, the lifetime of the POZ is about 90 ms for reaction with O_3 and 5 ms for reaction with H_2O. While hydrolysis still dominates the removal of POZ, some SOZ would be formed. The health effects of SOZ are not known. However, given that it is an oxidant and that the organic side chains will increase its solubility in lipids and cell membranes, it has the potential to negatively impact health. The same is true of the hydroxyhydroperoxide products of the POZ hydrolysis.

In agreement with the studies of Nizkorodov and coworkers,[72–74] the SOZ generated in the ozone–alkene reactions can clearly photolyze, and in this case, form anhydrides, acids and aldehydes. Their study also showed evidence of a rich chemistry resulting in the formation of complex oxygenated products on oxidized SAM surfaces. These products were photoactive in the tropospheric actinic window ($\lambda > 295$ nm) and released surface aldehyde, formic acid and other small molecules in the gas phase. The formation of formic acid in the present studies suggests that similar photochemistry occurs in part in the case of ozonized OPPC as well.

Acknowledgements

This study was supported by the National Science Fundation (grant CHE-0423804). This research was in part performed in the Environmental Molecular Sciences Laboratory, a national scientific user facility sponsored by the U. S. Department of Energy's Office of Biological and Environmental Research at Pacific Northwest National Laboratory (PNNL) and supported by the U. S. Department of Energy Office of Basic Energy Sciences, Chemical Sciences Division. PNNL is operated by the U. S. Department of Energy by Battelle Memorial Institute under contract #DE-AC06-76RL0 1830. We thank Dr Alexander Laskin and Huda Shaka' for performing SEM measurements. We are grateful to Dr John Greaves for his help in the interpretation of the MALDI spectra. Finally we want to thank Christopher Harmon for his help with the MALDI measurements and Professor Leon F. Phillips, Dr Theresa McIntire and Dr Yong Yu for helpful discussions.

References

1 D. C. Blanchard, *J. Geophys. Res.*, 1985, **90**, 961–963.
2 E. R. Lewis and S. E. Schwartz, *Sea Salt Aerosol Production: Mechanisms, Methods, Measurements and Models. A Critical Review*, American Geophysical Union, Washington, DC, 2005, vol. 152.
3 A. H. Woodcock, *J. Meteorol.*, 1953, **10**, 362–371.
4 A. H. Woodcock, *J. Geophys. Res.*, 1972, **77**, 5316–5321.
5 H. Tervahattu, K. Hartonen, V. M. Kerminen, K. Kupiainen, P. Aarnio, T. Koskentalo, A. F. Tuck and V. Vaida, *J. Geophys. Res.*, 2002, **107**.
6 H. Tervahattu, J. Juhanoja and K. Kupiainen, *J. Geophys. Res.*, 2002, **107**.
7 B. Alberts, D. Bray, J. Lewis, M. Raff, K. Roberts, J. D. Waston, The plasma membrane, in *Molecular Biology of the Cell*, Garland, New York, 1989, ch. 6.
8 G. B. Ellison, A. F. Tuck and V. Vaida, *J. Geophys. Res.*, 1999, **104**, 11633–11641.
9 R. B. Gagosian, E. T. Peltzer and O. C. Zafiriou, *Nature*, 1981, **291**, 312–315.
10 J. C. Marty, A. Saliot, P. Buatmenard, R. Chesselet and K. A. Hunter, *J. Geophys. Res.*, 1979, **84**, 5707–5716.
11 D. C. Blanchard, *J. Rech. Atmos.*, 1974, **8**, 529–539.
12 D. C. Blanchard and L. Syzdek, *Science*, 1970, **170**, 626.
13 S. Decesari, M. C. Facchini, S. Fuzzi, G. B. McFiggans, H. Coe and K. N. Bower, *Atmos. Environ.*, 2005, **39**, 211–222.
14 B. J. Finlayson-Pitts and J. N. Pitts, Jr, *Chemistry of the Upper and Lower Atmosphere—Theory, Experiments, and Applications*, Academic Press, San Diego, 2000.
15 S. J. Ghan and S. E. Schwartz, *Bull. Am. Met. Soc.*, 2007, **88**, 1059.
16 H. M. Hung and P. Ariya, *J. Phys. Chem. A*, 2007, **111**, 620–632.
17 A. Asad, B. T. Mmereki and D. J. Donaldson, *Atmos. Chem. Phys.*, 2004, **4**, 2083–2089.
18 M. P. Fuller and P. R. Griffiths, *Anal. Chem.*, 1978, **50**, 1906–1910.
19 P. R. Griffiths and M. P. Fuller, *Adv. Infrared Raman Spectrosc.*, 1982, **10**, 63–129.
20 R. Vogt and B. J. Finlayson-Pitts, *J. Phys. Chem.*, 1994, **98**, 3747–3755.
21 C. C. Lai, S. H. Yang and B. J. Finlayson-Pitts, *Langmuir*, 1994, **10**, 4637–4644.
22 M. L. E. Tevrucht and P. R. Griffiths, *Appl. Spectrosc.*, 1989, **43**, 1492–1494.
23 J. R. Yates, *J. Mass Spectrom.*, 1998, **33**, 1–19.

24 K. D. Childs, B. A. Carlson, L. A. LaVanier, J. F. Moulder, D. F. Paul, W. F. Stickle and D. G. Watson, *Handbook of Auger Electron Spectroscopy: A Book of Reference Data for Identification and Interpretation in Auger Electron Spectroscopy*, Physical Electronics, Eden Prairie, 3rd edn, 1995.
25 Q. Dai, J. Hu and M. Salmeron, *J. Phys. Chem. B*, 1997, **101**, 1994–1998.
26 M. Luna, F. Rieutord, N. A. Melman, Q. Dai and M. Salmeron, *J. Phys. Chem. A*, 1998, **102**, 6793–6800.
27 J. L. R. Arrondo, F. M. Goni and J. M. Macarulla, *Biochim. Biophys. Acta*, 1984, **794**, 165–168.
28 L. J. Bellamy, *The Infrared Spectra of Complex Molecules*, Chapman and Hall, London, 1980.
29 Y. Dubowski, J. Vieceli, D. J. Tobias, A. Gomez, A. Lin, S. A. Nizkorodov, T. M. McIntire and B. J. Finlayson-Pitts, *J. Phys. Chem. A*, 2004, **108**, 10473–10485.
30 B. J. Finlayson-Pitts, L. L. Sweetman and B. Weissbart, *Toxicol. Appl. Pharmacol.*, 1987, **89**, 438–448.
31 G. Socrates, *Infrared and Raman Characteristic Group Frequencies*, John Wiley & Sons, New York, 2001.
32 L. A. Hull, I. C. Hisatsune and J. Heicklen, *J. Am. Chem. Soc.*, 1972, **94**, 4856–4864.
33 U. Samuni, Y. Haas, R. Fajgar and J. Pola, *J. Mol. Struct.*, 1998, **449**, 177–201.
34 P. S. Bailey, *Ozonation in Organic Chemistry*, Academic Press, New York, 1978, vol. I.
35 R. Criegee, *Rec. Chem. Prog.*, 1957, **18**, 111–120.
36 J. C. Ewing, J. P. Cosgrove, D. H. Giamalva, D. F. Church and W. A. Pryor, *Lipids*, 1989, **24**, 609–615.
37 C. C. Lai, B. J. Finlayson-Pitts and W. V. Willis, *Chem. Res. Toxicol.*, 1990, **3**, 517–523.
38 O. S. Privett and E. C. Nickell, *J. Am. Oil Chem. Soc.*, 1964, **41**, 72.
39 J. N. Roehm, J. G. Hadley and D. B. Manzel, *Arch. Intern. Med.*, 1971, **128**, 88.
40 J. N. Roehm, J. G. Hadley and D. B. Menzel, *Arch. Environ. Health*, 1971, **23**, 142.
41 T. Moise and Y. Rudich, *J. Geophys. Res.*, 2000, **105**, 14667–14676.
42 E. R. Thomas, G. J. Frost and Y. Rudich, *J. Geophys. Res.*, 2001, **106**, 3045–3056.
43 W. A. Pryor, *Am. J. Clin. Nutr.*, 1991, **53**, 702–722.
44 S. D. Razumoskii and G. E. Zaikov, *Ozone and Its Reactions with Organic Compounds*, Elsevier, New York, 1984.
45 Y. Wadia, D. J. Tobias, R. Stafford and B. J. Finlayson-Pitts, *Langmuir*, 2000, **16**, 9321–9330.
46 S. Gäb, E. Hellpointer, W. V. Turner and F. Korte, *Nature*, 1985, **316**, 535–536.
47 S. Hatakeyama and H. Akimoto, *Res. Chem. Intermed.*, 1994, **20**, 503–524.
48 O. Horie, P. Neeb, S. Limbach and G. K. Moortgat, *Geophys. Res. Lett.*, 1994, **21**, 1523–1526.
49 J. Santrock, R. A. Gorski and J. F. Ogara, *Chem. Res. Toxicol.*, 1992, **5**, 134–141.
50 F. Sauer, C. Schafer, P. Neeb, O. Horie and G. K. Moortgat, *Atmos. Environ.*, 1999, **33**, 229–241.
51 R. Simonaitis, K. J. Olszyna and J. F. Meagher, *Geophys. Res. Lett.*, 1991, **18**, 9–12.
52 B. Teige, T. T. McManus and J. B. Mudd, *Chem. Phys. Lipids*, 1974, **12**, 153–171.
53 H. J. Tobias and P. J. Ziemann, *J. Phys. Chem. A*, 2001, **105**, 6129–6135.
54 U. P. Fingeli and H.H. Gunthard, Infrared membrane spectroscopy, in *Membrane Spectroscopy*, ed. E. G., Springer, Berlin, 1981, pp. 270–332.
55 W. Hübner and A. Blume, *Chem. Phys. Lipids*, 1998, **96**, 99–123.
56 R. Atkinson and S. M. Aschmann, *Environ. Sci. Technol.*, 1993, **27**, 1357–1363.
57 A. A. Chew and R. Atkinson, *J. Geophys. Res.*, 1996, **101**, 28649–28653.
58 B. J. Finlayson, J. N. Pitts, Jr and H. Akimoto, *Chem. Phys. Lett.*, 1972, **12**, 495.
59 J. A. Kroll, S. R. Sahay, J. G. Anderson, K. L. Demerjian and N. M. Donahue, *J. Phys. Chem. A*, 2001, **105**, 4446–4457.
60 P. Neeb and G. K. Moortgat, *J. Phys. Chem. A*, 1999, **103**, 9003–9012.
61 S. E. Paulson, M. Y. Chung and A. S. Hasson, *J. Phys. Chem. A*, 1999, **103**, 8125–8138.
62 S. E. Paulson, J. D. Fenske, A. D. Sen and T. W. Callahan, *J. Phys. Chem. A*, 1999, **103**, 2050–2059.
63 A. R. Rickard, D. Johnson, C. D. McGill and G. Marston, *J. Phys. Chem. A*, 1999, **103**, 7656–7664.
64 L. H. Cohen and A. I. Gusev, *Anal. Bioanal. Chem.*, 2002, **373**, 571–586.
65 D. J. Harvey, *Mass Spectrom Reviews*, 1999, **18**, 348.
66 M. J. Kang, A. Tholey and E. Heinzle, *Rapid Commun. Mass Spectrom.*, 2000, **14**, 1972.
67 M. Petkovic, J. Schiller, J. Muller, M. Muller, K. Arnold and J. Arnhold, *Analyst*, 2001, **126**, 1042–1050.
68 M. Hallquist, N. B. Petrucci, C. Kreuzer, V. P. Ostanin and R. A. Cox, *Phys. Chem. Chem. Phys.*, 2000, **2**, 4373–4378.
69 I. N. Tang and H. R. Munkelwitz, *Atmos. Environ.*, 1993, **27**, 467–473.
70 M. A. Shaw and M. J. Rood, *Atmos. Environ.*, 1990, **24**, 1837–1841.
71 J. M. Anglada, P. Aplincourt, J. M. Bofill and D. Cremer, *ChemPhysChem*, 2002, **3**, 215.
72 A. L. Gomez, J. Park, M. L. Walser, A. Lin and S. A. Nizkorodov, *J. Phys. Chem. A*, 2006, **110**, 3584–3592.
73 J. Park, A. L. Gomez, M. L. Walser, A. Lin and S. A. Nizkorodov, *Phys. Chem. Chem. Phys.*, 2006, **8**, 2506–2512.
74 M. L. Walser, J. Park, A. L. Gomez, A. R. Russell and S. A. Nizkorodov, *J. Phys. Chem. A*, 2007, **111**, 1907–1913.
75 L. R. Fiegland, M. M. Saint Fleur and J. R. Morris, *Langmuir*, 2005, **21**, 2660–2661.
76 P. R. Story, W. H. Morrison III, T. K. Hall, J.-C. Farine and C. E. Bishop, *Tetrahedron Lett.*, 1968, **29**, 3291–3294.
77 T. Carlson, *Photoelectron and Auger Spectroscopy*, Springer, New York, 1975.
78 J. Vieceli, O. L. Ma and D. J. Tobias, *J. Phys. Chem. A*, 2004, **108**, 5806–5814.
79 B. Mile, G. W. Morris and A. G. Alcock, *J. Chem. Soc., Perkin Trans. 2*, 1979, 1644–1652.
80 M. E. Jung and P. Davidov, *Org. Lett.*, 2001, **3**, 627–629.
81 B. de Foy, E. Caetano, V. Magana, A. Zitacuaro, B. Cardenas, A. Retama, R. Ramos, L. T. Molina and M. J. Molina, *Atmos. Chem. Phys.*, 2005, **5**, 2267.
82 J. Gasca, E. Ortiz, H. Castillo, J. L. Jaimes and U. Gonzalez, *Atmos. Environ.*, 2004, **38**, 3517.